

## Drying of a Compressible Biporous Material

T. Lerouge,<sup>1,2</sup> B. Mailliet<sup>1</sup>,,<sup>1</sup> D. Coutier-Murias<sup>1</sup>,,<sup>1</sup> D. Grande,<sup>2</sup> B. Le Droumaguet,<sup>2</sup> O. Pitois,<sup>1</sup> and P. Coussot<sup>1,\*</sup>

<sup>1</sup>Laboratoire Navier (ENPC-Univ Gustave Eiffel-CNRS), Champs sur Marne, France

<sup>2</sup>Univ. Paris-Est, ICMPE (UPEC-CNRS), Thiais, France

 (Received 29 November 2019; revised manuscript received 18 March 2020; accepted 30 March 2020; published 23 April 2020)

We study the consequences of drying on the internal structure of compressible materials containing pores of different sizes, which may be seen as model systems of sponges or wood. With the help of original techniques, we devise biporous media with different relative amounts of small and large pores, and follow the evolution of the liquid fraction simultaneously in each pore type. We show that in a compressible biporous medium with dispersed large pores (i.e., not directly connected) drying induces the homogeneous emptying of the large pores first, due to their compression, along with some compression of the small-pore matrix. In contrast, when the large pores are connected, they successively empty without compression. In both cases, the small pores start or finish to empty in the next stage, and a constant drying rate is observed during most of the time, thanks to liquid films maintaining the contact of the liquid network with the free surface of the sample.

DOI: [10.1103/PhysRevApplied.13.044061](https://doi.org/10.1103/PhysRevApplied.13.044061)

### I. INTRODUCTION

Many products (paper, textile, food, agriculture, chemicals, civil engineering, etc) are wet during their preparation so that they are easier to formulate, mix, handle, and transport. Then they need to be dried at some step of fabrication to end as solid materials easier to conserve or use. Besides, natural materials such as wood, plants, animal tissues, and soils, undergo imbibition-drying cycles, which can strongly affect their structure and their liquid-transport properties.

Drying mechanisms are relatively well known for simple incompressible homogeneous porous media (i.e., made of a fixed well-connected hydraulic network of similar local porous structures) filled with pure liquid [1–5]: in the absence of gravity effects, one observes first a more or less long constant- (drying) rate period (CRP), with a homogeneous desaturation of the medium thanks to capillary equilibration processes [4,6] keeping the Laplace pressure uniform throughout the liquid network and allowing for water redistribution throughout the medium; such a homogeneous desaturation is observed down to low saturation (defined as the liquid-to-pore volume ratio) in homogeneous media with pore size from several tens of microns [5,7–10] down to nanometers [5]; this is followed by a falling-rate period (FRP) associated with the development of a heterogeneous profile of saturation, due to a demand of liquid, through the imposed evaporation rate at the

free surface, larger than the liquid transport induced by capillary effects [5,11,12].

When the sample is made of two regions with different pore sizes, the region of largest pore size starts emptying first, whatever its location in the system. This leads to the spectacular emptying of a large-pore medium covered by a small-pore medium, while the latter remains apparently saturated (and the only one submitted to an air flux) [13, 14]: the air is conveyed through the small-pore medium by transient thin paths, which immediately close when they have reached the large-pore medium.

On the other hand, some solid structures cannot support the capillary pressure induced by air penetration, and tend to fracture or shrink. This is, for example, the case of gels [15], colloidal pastes [16,17], or clays [14]. This, for example, leads to wood collapse [18], creasing of elastomeric solids [19], or sponge shrinkage [20].

Complex materials with a compressible multiscale porous structure are nevertheless common: wood, sponges, soils, fresh cementitious pastes, aerated food pastes, etc. One may ask whether such materials will first fully shrink then let air penetrate or if some air can penetrate in the partially shrunk structure, or even not shrunk at all. This will obviously have a critical impact on the final state of the material after drying. This might, in fact, depend on some characteristics of the structure that need to be explored. As far as we know, only the case of composite systems (see above) has been studied, and no study has focused on the impact of several pore sizes on the drying characteristics of homogeneous materials. Here we intend to clarify the

\*Philippe.coussot@univ-eiffel.fr

possible interplay between shrinkage and air invasion in the structure of such systems during drying.

In order to understand the effect of a multiscale porosity on drying characteristics in terms of liquid distribution in time and possible shrinkage, we use a compressible “biporous” system, with mainly two pore sizes, with different relative fractions of these pores: from a homogeneous small-pore system (no large pores) to a homogeneous large-pore system (no small pores). We use nuclear magnetic resonance (NMR), which appears to be a powerful technique to get an idea of the evolutions of the internal characteristics at the pore scale during drying. We show that whatever the porous structure (connected or dispersed large pores in a matrix of small pores) the largest pores homogeneously fully drain first during the CRP, but the connectivity plays a critical role: large pores significantly shrink, except if they are connected.

## II. MATERIALS AND METHODS

### A. Materials

#### 1. Monoporous medium

The polymerization mixture, composed of 2-hydroxyethyl methacrylate (HEMA), ethylene glycol dimethacrylate (EGDMA) (with a molar ratio of 70:30 mol%) and 2,2-dimethoxy-2-phenyl acetophenone (DMPA) (2 wt% with respect to the total comonomer amount), is homogenized with 80 vol% i-PrOH (isopropanol) (with respect to the total volume of comonomers). This mixture is placed in a spectrolinker XL-1500 UV oven (Spectronics, Westbury, NY, USA) equipped with six lamps ( $6 \times 15$  W) for 4 h of irradiation at 365 nm so as to trigger the photoinduced free-radical copolymerization. The alcohol is then removed under vacuum overnight. The porosity of this medium is  $\varepsilon \approx 80\%$ .

#### 2. Biporous media

To obtain dispersed large pores, a given volume of roughly cubic NaCl particles are sieved between 250 and 400  $\mu\text{m}$ , then added to the above mixture, which is then continuously agitated by rotation during polymerization. Sedimentation is counterbalanced first by agitation, then

thanks to the viscosity increase during polymerization, which makes it possible to maintain a good dispersion of the NaCl particles. Different concentrations of particles can be obtained in this way by varying the suspended volume, up to the maximum packing fraction, but in any case the particles are not connected in the sense that two neighboring particles are always separated by a thin film of the polymeric mixture.

A network of connected large pores is obtained by submitting a simple particle packing either to oven sintering at 740  $^{\circ}\text{C}$  during 4 h, or to a spark-plasma-sintering (SPS) treatment (Sumitomo Dr Sinter Lab 515S machine from Fuji Electronic Industrial) at 100  $^{\circ}\text{C}$  during 20 min under a load of 50 kN. The liquid polymer mixture is then added within the sintered packing under a slight pressure, and polymerized.

Finally, both porogenic agents (salt + interstitial liquid) are removed by immersing the resulting materials in deionized water for 2 days with sintered particles and 4 days with dispersed particles, and the extraction solution is renewed twice a day. The materials are finally abundantly washed with deionized water, then dried under vacuum at room temperature overnight. The full removal of porogenic agents is checked by controlling that after stabilization the final mass of material is equal to the total mass of comonomers in the initial polymer mixture.

#### 3. “Macroporous” medium

In order to obtain a material with connected large pores within a nonporous matrix, a polymer mixture without i-PrOH, i.e., composed of only both comonomers and DMPA, is injected under reduced pressure inside a sintered NaCl packing, then submitted to UV irradiation. The salt is then removed by the above-described technique. The volume fraction of large pores in that case is around 80%.

#### 4. Gallery of material types

Some views of the different material types are shown in Fig. 1. The monoporous medium, the macroporous medium and the connected biporous system have been characterized in detail in Refs. [21,22]. In particular, mercury porosimetry shows (see Appendix A, Fig. 12) almost

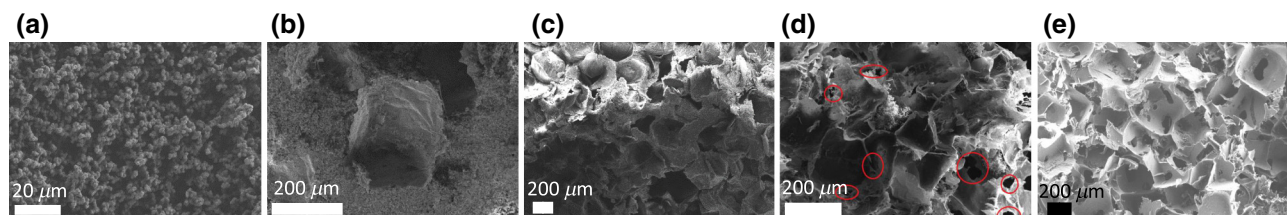


FIG. 1. Images of the different system types obtained from scanning electron microscopy: (a) microporous; (b) nonconnected biporous ( $n = 0.24$ ), (c) nonconnected biporous ( $n = 0.59$ ), (d) connected biporous ( $n = 0.81$ ), (e) macroporous. Red contours in (d) indicate interconnections between large pores. These interconnections are more directly visible (black holes) in (e).

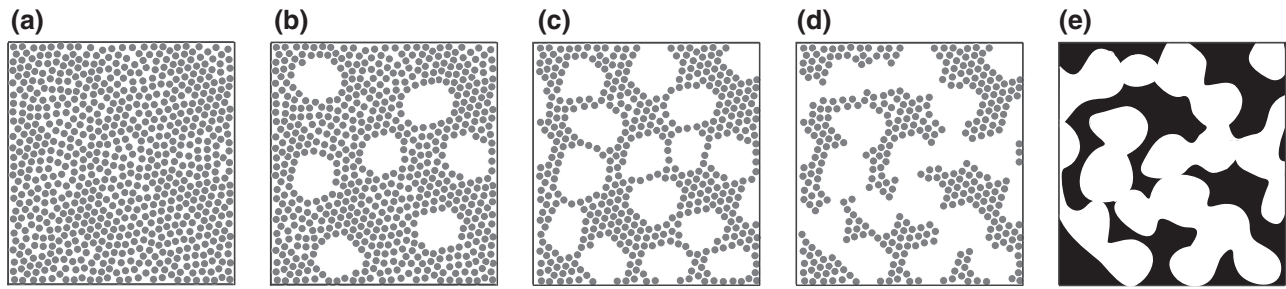


FIG. 2. Scheme of principle for the different types of biporous structures prepared in this study: homogeneous small-pore medium ( $n = 0$ ) (a), nonconnected large pores in a matrix of small pores (b,c), connected large pores embedded in the small-pore matrix (d), large pores without small pores ( $n = 1$ ) (e).

homogeneous pore distributions at  $5 \mu\text{m}$  for the monoporous medium, and at  $100 \mu\text{m}$  for the macroporous medium, while the connected biporous system essentially exhibits these two pore sizes, as expected. Note that the  $100\text{-}\mu\text{m}$ -sized porosity level corresponds to the diameter of the interconnections between adjacent pores [see Figs. 1(d) and 1(e)], due to the threshold size theory. Considering the characteristics of the monoporous medium we consider it as a homogeneous small pore system and refer to it as a “microporous medium.”

The different medium types obtained finally cover the different possible configurations of a porous system including two sizes of pores: no large pores (i.e., homogeneous small- (connected) pore medium [Fig. 2(a)]); dispersed (i.e., not directly connected) large pores [Fig. 2(b)], high concentration of large pores [Fig. 2(c)], or connected large pores [see Fig. 2(d)], in a small-pore matrix; only large pores in a nonporous matrix [Fig. 2(e)]. These different structures are described by means of the parameter  $n$ , defined as the initial ratio of large pores to the total pore volume.

Note that some thin films apparently form around the salt inclusions during the polymerization [see [22] and Figs. 1(b)–1(d)]. It is worth emphasizing that these films are porous and/or do not cover all the large-pore interface since the removal of salt, initially in the inclusions, can be achieved relatively rapidly (see preparation procedure) by simple diffusion in water from the interior of the sample. Moreover, as we see below, during drying, the transport of liquid from the large pores to the sample surface, through the microporous matrix, does not seem to be perturbed by these films, since for dispersed inclusions we observe a full removal of this water along with a constant drying rate. This justifies the fact that we neglect the presence of these films in the detailed discussion of results.

### 5. Mechanical characteristics of the samples

The samples are deformable and compressible. In order to appreciate their ability to deform when submitted to some stress we simply carry out compression tests. The

test consists of placing a cylindrical sample between two solid plates, which are then progressively approaching each other while the normal force is measured. The material is initially water saturated. The normal stress (force and sample cross-section area) versus deformation (vertical displacement and initial sample height) curve can then be drawn (see Fig. 3).

From these data it appears that the macroscopic medium requires high stress to be significantly deformed, which is due to its plain solid polymeric structure. In contrast, the microporous medium may be significantly deformed under lower stress, thanks to a large porosity (80%) and a structure of polymer aggregates with weak links, which can easily move relative to each other leading to deformation or shrinkage. At last, a connected biporous system even more easily deforms under some stress as its mechanical strength relies on a thin deformable microporous matrix. A nonconnected concentrated biporous medium behaves in the same way. A dispersed biporous medium is obviously expected to behave in an intermediate way between the pure microporous medium and the connected biporous system. We do not present more precise information on

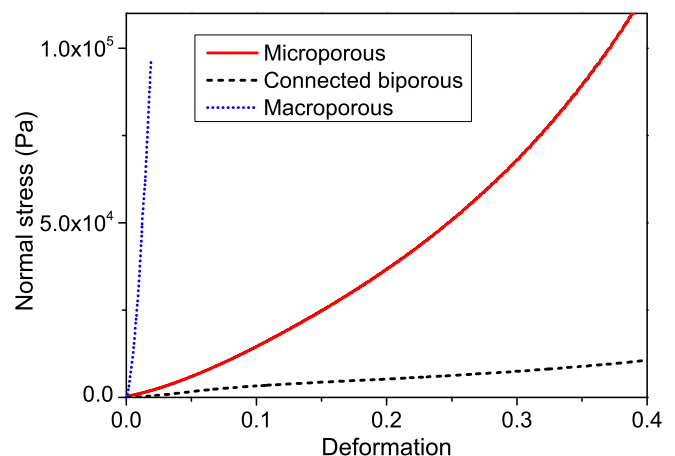


FIG. 3. Normal stress versus deformation during a compression test for different sample types.

the latter point as in the present study we only discuss qualitatively its impact on the drying characteristics.

At last note that it has been shown [23] that the (non-porous) polymer matrix does not swell or adsorb water, even over long times. Moreover, the wetting characteristics of the polymer matrix have been studied in depth in Ref. [22]. The contact angle of water on the polymer lies in the range  $40^{\circ}$ – $45^{\circ}$ .

## B. Drying characteristics' determination

### 1. Experimental procedure

In order to follow the drying characteristics of our media we insert each sample in a Bruker NMR spectrometer, 0.5 T, and impose a dry-air flux perpendicular to the sample free surface. The cylindrical sample (diameter either equal to 12 or to 16 mm) is placed in a glass cylinder, which, due to shrinkage, may leave a gap of up to 1 mm between the sample and the cylinder walls. This distance remains nevertheless much smaller than the sample height ( $>1$  cm). Under such conditions, even if the peripheral surface of the sample is wet, the relative humidity in this small gap remains maximum along most of the sample height, so that vapor diffusion is negligible and so is evaporation from the peripheral surface of the sample. This effect was, for example, demonstrated by numerical simulation in the case of a long rectangular channel [24]: the relative humidity significantly differs from 1 around the channel exit, so that evaporation can occur only in this region.

We measure the NMR relaxation through a Carr-Purcell-Meiboom-Gill (CPMG) sequence composed of a first  $\pi/2$  pulse and 2000  $\pi$  pulses during 5000 ms distributed in logarithmic intervals. The repetition time is 10 s to get a complete relaxation of all protons. This sequence is repeated four times to increase the signal-to-noise ratio. The  $T_2$  distribution can then be resolved by means of inverse Laplace transform (ILT). Our procedure is a non-negative least-squares fit to the data with Tikhonov regularization, which is similar to the ‘‘Contin’’ method [25,26] and described in Ref. [27]. We finally get an apparent statistical distribution of  $T_2$ , expressed in terms of signal intensity associated with each possible value of  $T_2$ , which we call ‘‘T distribution’’ in the following. Note that the exact shape of this T distribution depends on the technique of regularization used, and in particular on the value of the ‘‘parsimony factor’’ [27]. However, the positions of the peaks and the amount of liquid associated with these peaks are robust values. Also, the evolution of the shape of the distribution is reliable information that can be used for a physical analysis of a set of data, as long as the parsimony factor is kept constant for the treatment of all these data.

Roughly speaking the relaxation time is related to the mobility of water molecules, and specific interactions of water with their environment (e.g., adsorption, proton exchange with other species, or magnetic interactions

at nanoscale). In the particular case of water embedded in a pore cavity, within the usual hypothesis of biphasic fast exchange [28], the relaxation time scales as the ratio of the volume of free liquid water to the area of the water-solid interface, with a factor depending on the NMR surface relaxivity. Note that this volume-to-surface ratio is proportional to radius in the case of uniform spherical pores.

Each of the T distribution may be analyzed by taking into account that the liquid in the large pores, if filled with liquid, has a relaxation time around 1000 ms, while the liquid in smaller pores has a much smaller relaxation time, typically around 150 ms. Although we cannot predict the exact values of relaxation time in each pore size without knowing the relaxivity of the medium, the former value is of the same order as the typical values of relaxation time of pure water in large volumes (a few seconds), and the latter value is consistent with the decrease induced by a much smaller volume-to-surface ratio in the small pores [29]. As a consequence, the amount of liquid in the large pores may be estimated from the integral of the T distribution around the peak for the largest  $T_2$ , while the amount of liquid in the small pores is estimated from the integral over the rest of the distribution. The total liquid amount can be computed from the sum of the two above values. For our materials, this approach is valid because there is no overlap of the effective distributions of two pore size types and the relaxation times associated with each pore size are very different, leading to quite distinct peaks in the distribution. However, if the large pores desaturate or shrink, the ratio of the area of the solid-liquid interface to the liquid volume increases. In that case, the remaining liquid (possibly in the form of films along the pore walls) exhibits a smaller relaxation time, which may ultimately approach that of the liquid in the small pores. Moreover, when the relaxation time of the liquid in the large pores starts to decrease so that the corresponding peak in the T distribution approaches the peak associated to small pores, they start to overlap so that it is more difficult to determine the amount of liquid in each region [27]. Thus, the T distribution provides information concerning the distribution of liquid blob sizes in each type of pore, through the position of the peak and the curve width around it, but the above effects may complicate the quantitative analysis. In the following we always *a priori* compute, the apparent liquid volume in the large pores from the integral of the curve around the peak associated to the largest relaxation time, and the apparent liquid in small pores from the rest of the distribution. Then, to describe the effective liquid transfers during the evolution of the T distribution along drying, we use these results and discuss their origin by taking into account the specificities of each situation.

Actually, a few ideal conditions of water extraction from the pores can be considered along with their impact on the T distribution. These situations serve as references for the

discussion of the data. In each case the integral of the signal decreases in time, as there is a net water removal from the porosity. A homogeneous shrinkage of the pores, or a homogeneous desaturation of the pores induces a decrease of the relaxation time in the form of a shift of the T distribution towards low values [see Fig. 4(a)]. A heterogeneous emptying of the pores does not induce any change of the T distribution except that the signal amplitude decreases [see Fig. 4(b)]. A heterogeneous desaturation of the pores leads to a spreading of the T distribution towards low values keeping constant its upper boundary [see Fig. 4(c)].

## 2. Structure characteristics

We recall the basic geometrical characteristics of the structure, i.e.,  $n$ , the ratio of large-pore volume ( $\Omega_1$ ) to the total pore volume at the initial time ( $\Omega_p = \Omega_1 + \Omega_2$ , where  $\Omega_2$  is the initial small-pore volume), i.e., before drying. These characteristics may nevertheless change during drying if some contraction of the pores occurs. On the other hand, the above analysis of NMR measurements allows determination of the liquid fraction in each pore type, defined as the ratio of the current liquid volume in this pore type to the total initial liquid volume ( $\Omega_L$ ) in the pores. Note that initially  $\Omega_p = \Omega_L$  since the medium is saturated. We can thus define  $\psi_1$  as the ratio of the current liquid volume in the large pores to  $\Omega_L$ , and  $\psi_2$  as the ratio

of the current liquid volume in the small pores to  $\Omega_L$ . We also define  $\psi$  as the ratio of the current total liquid volume in all pore types to  $\Omega_L$ . As a consequence we have  $\psi = \psi_1 + \psi_2$ . Note that, by definition, since the material is initially saturated, we have  $\psi_1(t=0) = \Omega_1/\Omega_p = n$ ,  $\psi(t=0) = 1$  and  $\psi_2(t=0) = \Omega_2/\Omega_p = 1 - n$ . Also remark that usually the evolution of liquid content in porous media is basically described with the help of the saturation, i.e., the ratio of liquid volume to the total pore volume. However, here, due to the possibility of contraction of the sample, this parameter does not inform us about the liquid loss, and  $\psi$  does not necessarily correspond to the saturation of the porous medium.

In order to follow the possible contraction of the sample we take photos along one radial direction at different times during drying in the same cylinder but outside the NMR apparatus. We then measure the apparent sample diameter at different heights and the sample height. The sample volume  $\Omega$  at each time is then estimated from the apparent average section (assuming a cylindrical shape) times the current height. Note that we observe essentially a homogeneous shrinkage (see Appendix B, Fig. 13) during the CRP. These measurements make it possible to determine at each time the apparent contraction, defined as the ratio of the current apparent volume of the sample to the initial one ( $\Omega_0$ ), i.e.,  $\tau^* = (\Omega_0 - \Delta\Omega)/\Omega_0$ , in which  $\Delta\Omega$  is the sample volume loss. From this value we can determine the contraction ratio of the volume of the pores (filled with liquid and/or air), defined as  $\tau = (\Omega_p - \Delta\Omega)/\Omega_p$ , where we recall that  $\Omega_p$  is the initial pore volume. Note that we have  $\Omega_0 = \Omega_p + \Omega_S$ , in which  $\Omega_S$  is the solid volume in the sample. Thus we can rewrite  $\tau$  as  $\tau = 1 - (1 - \tau^*)/(1 - \Omega_S/\Omega_0)$ . Using the definition of the initial porosity of the microporous matrix, i.e.,  $\varepsilon = \Omega_2/(\Omega_2 + \Omega_S)$ , and the various above expressions, we can deduce  $\Omega_S/\Omega_0 = (1 - n)/(1 + \eta - n)$  with  $\eta = \varepsilon/(1 - \varepsilon)$ , from which we can compute  $\tau$ . Note that in the absence of air penetration in the porous medium the sample volume loss  $\Delta\Omega$  is equal to the liquid volume loss, so in this regime we have  $\tau = \psi$ . In practice,  $\varepsilon$  can be determined from density measurements [22],  $\tau^*$  is directly measured from apparent volume variation as above described, and  $n$ ,  $\psi_1$  and  $\psi_2$  can be determined from the T distributions in time.

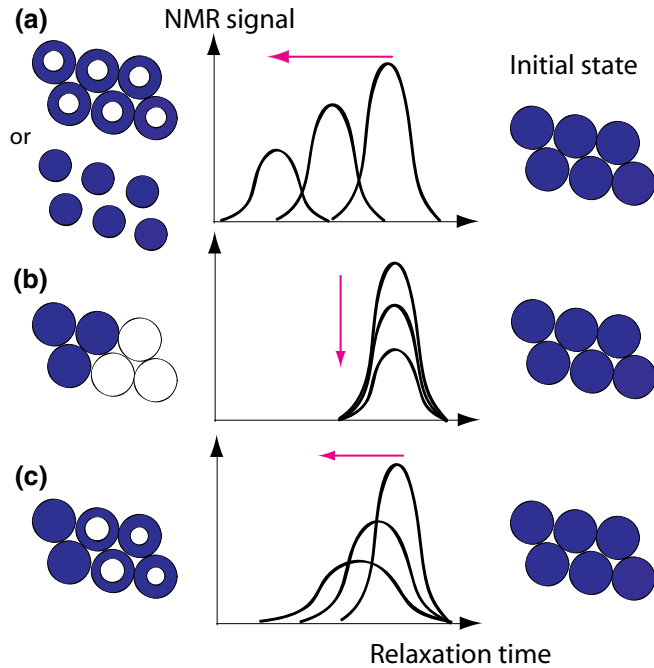


FIG. 4. Evolution of the T distribution in different ideal cases of water extraction from pores [disks initially filled with water (in blue)]: (a) homogeneous pore shrinkage or pore desaturation, (b) heterogeneous pore emptying, (c) heterogeneous pore desaturation.

## III. RESULTS AND DISCUSSION

### A. Generalities

For all our media we observe a long CRP during which  $\psi$  decreases linearly in time, followed by a FRP starting when  $\psi$  reaches about 0.1 typically (see Figs. 2–5). Since the drying rate also corresponds to the flux of vapor through the (top) free surface of the sample, which results from vapor diffusion, a constant value implies that the distribution of relative humidity (related to the distribution of vapor density) is constant in this region. This result

can be understood only if maximum relative humidity is maintained around the sample free surface during the CRP. Moreover, this region can be kept wet only thanks to a constant supply of liquid from the interior of the sample. At this stage, it should be said that, in the porous network, gravity effect induces pressure of the order of 100 Pa, while the capillary pressure is a hundred times larger. Therefore, the liquid transfer discussed above results from capillary processes throughout the sample, while evaporation inside the medium is negligible. Since drying under convection is in general relatively slow, these capillary effects allow a uniform saturation to be maintained throughout the sample during the CRP for homogeneous media with a (“single”) pore size in a wide range [5]. In our case, i.e., for biporous systems, we see that most interesting effects in our context occur during the CRP, a period during which capillary effects govern the liquid distribution inside the medium. As a consequence, as long as we focus on the CRP, the drying-rate value has no impact on the mechanisms observed here, so we can compare their evolution by rescaling time by the characteristic duration of the CRP, i.e.,  $\theta = \psi^{-1}$ , which is measured to be in the range 1.5–8 h. We can suggest that such a large range of values, although the global air-flux conditions remain constant, results from the sensitivity of the evaporation rate to the exact boundary conditions along the sample free surface. More precisely, describing the drying rate with the help of the standard approach of vapor diffusion through a boundary layer of thickness  $\delta$  above the free surface (see [5]), we find, for example when the CRP duration is 2 h for a sample of height 1 cm, that  $\delta$  should be equal to 500  $\mu\text{m}$ . In reality, this scheme is perturbed by the roughness of the sample free surface, and by the development of a thin dry layer at the sample top, through which the vapor has now to diffuse to reach the sample free surface. The latter effect can, in particular, be very significant, for example, with a macroporous system made of large inclusions of several hundreds of  $\mu\text{m}$  diameter, as the dry top surface might be of the order of a few hundreds of  $\mu\text{m}$  thick. This may be further discussed, in particular, taking into account the specificities of the diffusion through the dry porous layer, for example, as in [5]. However, we do not have sufficient information on the local characteristics of drying (i.e., liquid distribution around the free surface) to properly discuss the validity of the scheme proposed. Also, this seems out of the scope of the paper, which focuses on bulk characteristics during the CRP, and all the discussion of the mechanisms identified below relies on the constancy of the drying rate in the CRP, without the need to know the exact drying rate during the CRP.

### B. Drying of a homogeneous small pore system (“microporous medium”)

Let us start by looking at the drying characteristics of the simplest case, i.e., the homogeneous microporous system.

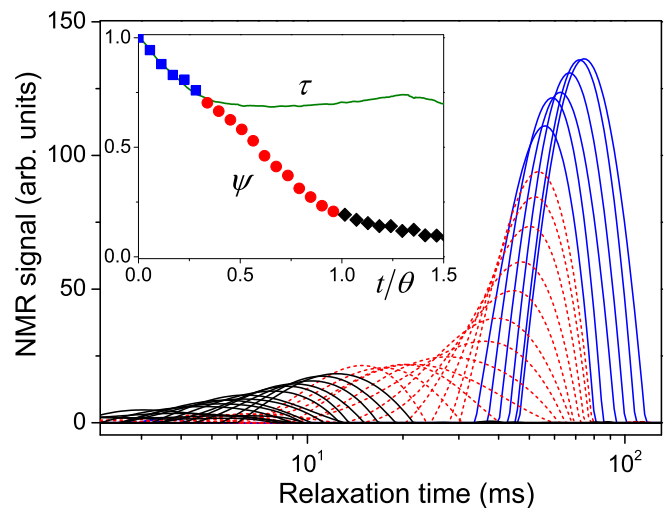


FIG. 5. Drying of a homogeneous medium with small pores [see Fig. 2(a) for an illustration]: relaxation time distributions at different successive times (every 21 min) (from right to left) during drying. The inset shows the liquid fraction and the liquid-phase contraction rate as a function of the dimensionless time ( $\theta = 22100$  s). Three regimes are identified: sample contraction (blue continuous lines and squares), homogeneous air penetration (red dashed line and circles), dry front development (black continuous lines and diamonds).

First of all, we observe that, as expected, the apparent saturation decreases linearly in time during a first stage. This is the CRP, during which the saturation should decrease homogeneously throughout the medium. Then we remark that at the beginning of this CRP, the T distribution essentially shifts (i.e., its width in a logarithmic scale does not change) towards lower T values while its amplitude decreases (see Fig. 5). This indicates [see Fig. 4(a)] a (spatially) homogeneous decrease of the relaxation time, otherwise the upper bound of the distribution in this region will remain fixed to account for regions remaining intact (i.e., keeping their initial relaxation time). This confirms a homogeneous desaturation of the sample.

If we now look at the contraction ratio, we see that during this phase it also linearly decreases, at the same rate as the apparent saturation (see inset of Fig. 5). This means that no air penetrates the sample during this phase, the pores are simply compressed to evacuate water. This is consistent with the observation that the T distribution is shifted towards lower relaxation time while its amplitude decreases: whatever the shape of the pore during this compression the volume-to-surface ratio decreases. This shrinkage is induced by the surface tension forces acting at each pore of the material’s peripheral surface, until the liquid-gas interface passes through those pores. The corresponding stress can be referred to as the breakthrough capillary pressure. The respective magnitudes of both this pressure and the elastic stress opposed by the material

set the shrinkage ratio. This analysis is consistent with our results. Indeed, the breakthrough capillary pressure is of the order of  $\sigma/R$  where  $\sigma$  is the surface tension (i.e., 0.07 N/m) and  $R$  the pore radius. Here we have  $\sigma/R \approx 30000$  Pa. According to the stress versus deformation curve for this material type (see Fig. 3), such a stress value can induce a deformation of the order of 0.2. This value is in the same order as the maximum deformation undergone by the sample during drying, i.e., around 0.25 (see inset of Fig. 5).

At the end of this period the contraction stops and we get back to the standard case of the drying of an incompressible homogeneous porous medium, with air penetrating to replace water drained towards the sample top surface, which results in a constant drying rate. During that stage, despite the fact that the drying rate is constant, so that *a priori* the desaturation is homogeneous for this medium, which resembles a granular packing, there is a first short period where the T distribution spreads towards lower  $T_2$  values, while the upper bound remains almost constant (say, the first six red dotted lines in Fig. 5), as in the ideal case shown in Fig. 4(c). This can be attributed to the fact that the distribution of air is here not homogeneous at some local scale: due to the complex liquid-air interface network formed throughout the sample (see below), partially empty pores can still be in contact with filled pores. In the next stage of the same regime (next dotted red lines in Fig. 5), i.e., last stage of the CRP, the T distribution continues spreading towards lower values while the upper bound significantly shifts towards lower values too, suggesting that all pores are now at least partially empty [cf. the ideal representation in Fig. 4(a)]. Note that there is a slight relaxation of the contraction as long as air penetrates and finally a slight further contraction in the FRP (see inset of Fig. 5) as some fully dry region grows from the sample top.

### C. Connected large pores in a nonporous matrix (“macroporous medium”)

In that case we observe essentially a decrease of the peak in the T distribution associated with liquid in large pores (around 1000 ms) (see Fig. 6), which obviously reflects the progressive disappearance of liquid in the large pores. However, remarkably, the average position (relaxation time) and width of this peak only slightly vary [as in the case of Fig. 4(b)], as compared to the large variations of one or both of these characteristics observed for the homogeneous microporous system in the different regimes (see Fig. 5). This suggests that the large pores do not progressively empty homogeneously throughout the sample, but instead successively empty, so that the remaining filled large pores still provide an NMR signal with this same high relaxation time. The successive emptying

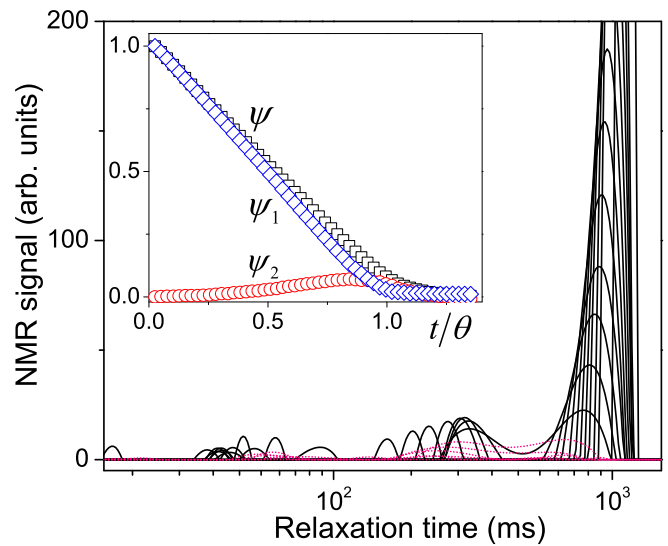


FIG. 6. Drying of a large connected pore medium [see Fig. 2(e) for an illustration]: relaxation time distributions at different successive times (every 7 min) (from right to left) during drying, first as black continuous lines, then as pink dotted lines from the last distribution reflecting liquid in large pores. For the sake of clarity only one in three measured distributions is represented. The inset shows the liquid fractions of the different regions (black squares for the total liquid fraction, blue diamonds for the liquid fraction in large pores, red circles in small pores) as a function of the dimensionless time ( $\theta = 5350$  s).

of large pores nevertheless leaves some liquid films or blobs along the walls. We effectively observe at the same time, some signal associated with much larger surface-to-volume ratios (i.e., situated at much smaller  $T_2$  values), which grows in time (see inset of Fig. 6). Since here there are no small pores, this signal likely finds its origin in some liquid films remaining along the previously emptied pores, and ensuring the hydraulic connection between filled pores and the free surface of the sample. Such a connection is indeed necessary to ensure a constant drying rate [30]. Although here the shape of the hydraulic network is more complex, the drying process observed is finally similar to the drying of a single channel (filled with liquid) taking the form of a progressive penetration of a large air finger leaving liquid films behind along some channel walls [24,31,32]. In that case the CRP lasts as long as the liquid films exist and can transport liquid sufficiently rapidly with regards to the rate of evaporation imposed along the sample free surface.

The sample contraction during this test was negligible, which is consistent with material characteristics. Indeed, here the breakthrough capillary pressure is of the order of 1400 Pa, which according to the stress versus deformation curve for this material type (see Fig. 3), can induce a deformation of the order of 0.001.

#### D. Origin of the differences in drying characteristics between the microporous and the macroporous systems

Although drying highlights a constant rate for both monoporous (microscopic and macroscopic) systems, the desaturation processes strongly differ. This is mainly due to differences observed for their respective porous structures. The liquid network of the large pore structure is made of enclosed volumes connected to a few neighbors by openings smaller than the pore size (see Sec. 2). In that case, drying essentially leads to the successive penetration of air in the connected pores, according to an invasion-percolation process [33–36]. More precisely, at the first step, drying leads to the extraction of liquid from a large pore, resulting in the formation of a liquid-air interface of the growing radius of curvature, so the pore partially empties but the interface cannot enter the neighboring pore due to the small radius curvature associated to it. Next pore invasion can be achieved only when the saturation of the large pore is sufficiently small, leading to liquid films with appropriate shapes. After some critical penetration a fast capillary-induced transfer occurs between the connected pores. Note that the newly invaded pore is the one having the largest opening with the first pore. In the next step the air volume grows again, now in both pores, until the interface finally penetrates a neighboring pore with the largest opening, and so on. This leads to an air path of complex shape, propagating essentially downwards through the structure [37]. As long as liquid films exist along the walls during this process the liquid is drained towards the sample free surface where it evaporates [9,24,38], which leads to constant drying rate. During this regime the number of almost empty pores increases in time, so does the amount of liquid films.

In contrast, the small pore system desaturates similarly to a granular packing, leading to a widely connected liquid network, which may be roughly seen as a three-dimensional net with uneven thickness of the threads and multiple connections in all directions. Such a structure does not allow the existence of well-identified enclosed pores. Under such conditions, a distribution of liquid-air interface may form throughout the medium with a relatively small curvature. Moreover, a significantly different distribution with a slightly larger curvature may be associated with a slightly smaller saturation. This explains that in a granular packing, a perfectly homogeneous desaturation is observed after the very first times of drying and during all the CRP [5]. Such a homogeneous desaturation enables maintaining a constant drying rate over the period.

#### E. Biporous system with connected large pores

Let us now consider a system similar to the macroporous system in terms of structure and distribution of

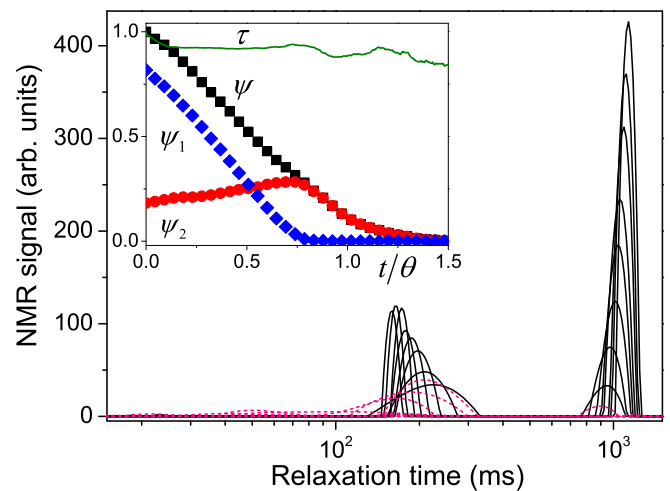


FIG. 7. Drying of a connected biporous system [see Fig. 2(d) for an illustration]: relaxation time distributions at different successive times (every 25 min) (from right to left) during drying, first as black continuous lines, then as pink dashed lines from the last distribution reflecting liquid in large pores. For the sake of clarity only one of the two measured distributions is presented. The inset shows the liquid fractions of the different regions (black squares for the total liquid fraction, blue diamonds for the liquid fraction in large pores, red circles in small pores) and the liquid-phase contraction rate (green continuous line) as a function of the dimensionless time ( $\theta = 16150$  s).

the large pores, but now with the solid matrix replaced by a microporous medium. Then, we observe the same main mechanism as for the simple macroporous system: the peak associated with large pores progressively disappears but keeps almost constant position and width (see Fig. 7), as in Fig. 4(b). In the meantime, the peak associated with the liquid in the small pores significantly varies: it progressively grows and shifts towards larger relaxation times (see Fig. 7). These different observations suggest an internal mechanism analogous to that observed for the simple macroporous system: a progressive inward penetration of air fingers leaving behind them, along the porous walls, liquid films, whose volume now contributes to the total NMR signal associated with small pores. After the full emptying of the large pores, the liquid films and the liquid in the microporous matrix progressively disappear (see Fig. 7). Finally, in that case, the microporous matrix does not significantly modify the internal drying mechanism as compared to the simple macroporous system, it just allows liquid to be stored temporarily, which then disappears during the end of the CRP and the FRP. It is to say that our measurements correspond to the “instantaneous” spatial distribution of liquid in the sample, so they do not provide any information about the potential contribution of the microporous matrix to transport liquid towards the sample free surface.

For this material type a slight contraction may be observed, typically of a few percent (see Fig. 3), which is in agreement with the above analysis. Indeed, here the breakthrough capillary pressure is associated with the air penetration in the large pores, so that we have 1400 Pa. According to the stress versus deformation curve for this material type (see Fig. 3), such a stress value can induce a deformation of the order of 0.05.

**F. Nonconnected large pores in a microporous matrix (large concentration)**

Let us now consider a system close to the previous one but with nonconnected large pores dispersed in a microporous matrix. The volume fraction of large pores is now slightly below the maximum packing fraction (i.e., about 64%). From the T distribution shown in Fig. 8 we clearly see that, in a first stage, the curve part associated with large liquid volumes disappears progressively while the distribution associated with the small pores is only essentially slightly deformed. The signal integral confirms that the large pores tend to drain first, well before the end of the CRP (see inset of Fig. 8). On the other hand, the small pores somewhat slowly drain during this first phase, and finally more rapidly drain when no more liquid is contained in large pores (see Fig. 8). Finally the T distribution in the large pore region is essentially shifted and somewhat expanded towards significantly lower relaxation times (see inset of Fig. 8), as in Fig. 4(a). The average relaxation time of the T distribution of the large pores typically decreases by a factor 2 during this process. This has two important implications: (i) the large pores drain homogeneously throughout the sample, i.e., all large pores start to drain approximately at the same time, otherwise the higher bound of the distribution will remain fixed, thus reflecting the fraction of large pores still filled; (ii) these pores drain progressively in time, since the T distribution progressively shifts towards lower relaxation times reflecting smaller volume-to-surface ratio of the liquid blobs. Thus we can conclude that the drying induces a progressive and homogeneous extraction of the liquid from the large pores throughout the medium. In the next stage, i.e., when the large pores are empty, the remaining T distribution (i.e., associated with small pores) starts to spread and shift towards lower T values, which is the hallmark of a homogeneous decrease of the saturation inside these pores.

If we now look at the liquid-phase contraction ratio (inset in Fig. 8), we see that it follows rather closely the apparent saturation. This means that the large-pore draining is essentially the result of their compression.

Considering these results, it is interesting to remark the large difference between the mechanisms for the connected and nonconnected large pores. In the former case there is

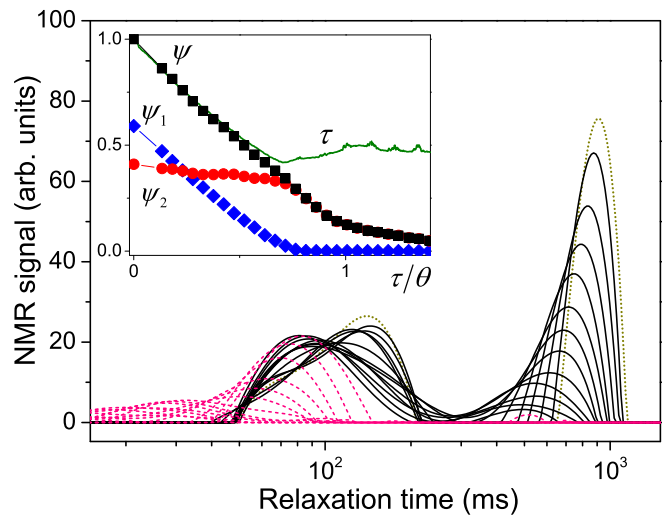


FIG. 8. Drying of a biporous medium [ $n = 0.59$ , see Fig. 2(c) for an illustration]: relaxation time distributions at different successive times (every 13 min) (from right to left) during drying, first as black continuous lines, then as pink dashed lines from the last distribution reflecting liquid in large pores. The initial curve is drawn as a dotted line. The inset shows the liquid fractions of the different regions (black squares for the total liquid fraction, blue diamonds for the liquid fraction in large pores, red circles in small pores) and the liquid-phase contraction rate (green continuous line) as a function of the dimensionless time ( $\theta = 17800$  s).

only a slight deformation induced by drying, the air penetrating progressively in the large pores first, which induces relatively low breakthrough capillary pressure. In the latter case, although the concentration of large pores is slightly lower, there is a large deformation of the system associated with the almost full compression of the large pores, so during the whole phase of drainage of the large pores there is almost no air penetrating the sample. This large compression results from the fact that, before it can invade the large pores, the air has now to go through the interstitial microporous matrix, thus inducing a large breakthrough capillary pressure associated with small pores, i.e., in the order of 30 000 Pa. On the other hand, since the material is soft (see Fig. 3), this can induce a large deformation. In practice this will fully shrink the large pores and ultimately partially shrink the microporous matrix.

**G. Nonconnected dispersed large pores in a microporous matrix**

As shown in Figs. 9 and 10 for smaller initial values of  $n$ , i.e., for dispersed large pores in the microporous matrix, the large pores still drain first while the small pores also slowly drain. In a second step the small pores go on draining at a higher rate, i.e., the drying rate of the CRP imposed to the whole sample. During the first stage a significant

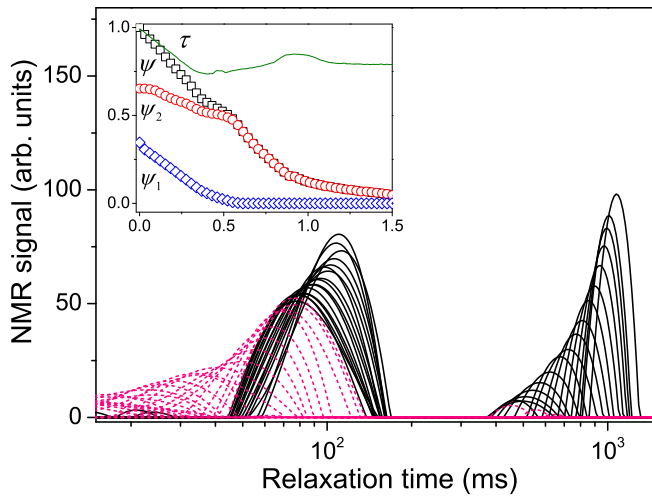


FIG. 9. Drying of a biporous medium [ $n = 0.34$ , see Fig. 2(b) for an illustration]: relaxation time distributions at different successive times (every 14.5 min) (from right to left) during drying, first as black continuous lines, then as pink dashed lines from the last distribution reflecting liquid in large pores. The inset shows the liquid fractions of the different regions (black squares for the total liquid fraction, blue diamonds for the liquid fraction in large pores, red circles in small pores) and the liquid-phase contraction rate (green continuous line) as a function of the dimensionless time ( $\theta = 28400$  s).

contraction occurs, but it is incomplete: it does not account for the whole water mass extraction and ends before the large pores are fully drained (see inset of Figs. 9 and 10). This means that for such materials, during the first stage, we should have not only some contraction of the large pores, but also some air penetration.

This may be explained by the fact that now the large pores can only partially shrink when they are dispersed in a microporous matrix. Indeed, for a concentrated system, a simple deformation (without significant compression) of the microporous thin layers around the large pores is likely sufficient to allow for the full shrinkage of the large pores. The deformation of thicker layers of microporous medium surrounding the large pores in a dispersed system is more difficult, and certainly requires some contraction of the microporous medium too. For example, the elastic buckling pressure of spherical pores of radius  $R$ , surrounded by a layer (thickness  $e$ ) of medium with elastic modulus  $E$ , evolves as  $P_b \approx Ee^2/R^2$  [39]. Thus we can expect that during this first stage both pore types contract, but at some time, the structure, which has been reinforced by the small pore contraction, does not allow further shrinkage of the large pores. Then the large pores have to drain while keeping the shape they have reached at the end of the contraction phase, and during this period the small pores are saturated (i.e., no air entrance) because capillary effects imply emptying first the largest pores. In

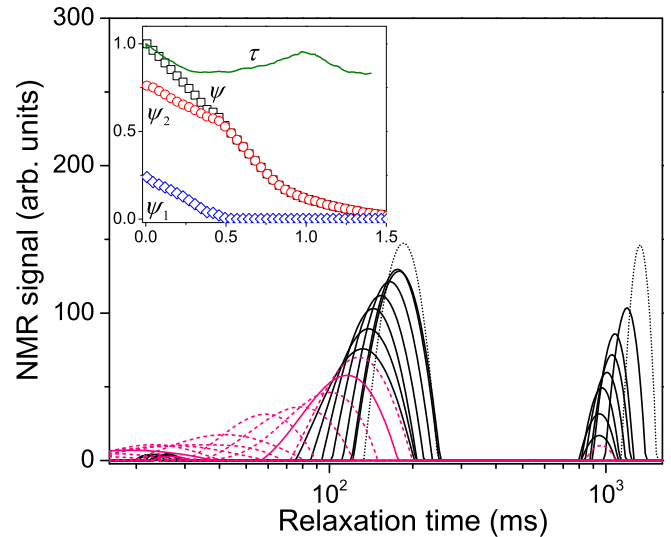


FIG. 10. Drying of a biporous medium [ $n = 0.24$ , see Fig. 2(b) for an illustration]: relaxation time distributions at different successive times (every 14.5 min) (from right to left) during drying, first as black continuous lines, then as pink dashed lines from the last distribution reflecting liquid in large pores. The initial curve is drawn as a dotted line. For the sake of clarity only one in two distributions is represented except for the two first distributions. The inset shows the liquid fractions of the different regions (black squares for the total liquid fraction, blue diamonds for the liquid fraction in large pores, red circles in small pores) and the liquid-phase contraction rate (green continuous line) as a function of the dimensionless time ( $\theta = 20700$  s).

the next stage, the contraction ratio increases (see insets of Figs. 9 and 10), an increase that ends approximately at the transition to the FRP. We have no explanation for this last effect at this stage; this is left for future work.

## H. Synthesis diagram

We now gather in the same plot the data for the evolution of the liquid fractions in the small pores and the total liquid fraction for the different systems containing large pores (see Fig. 11). The total liquid fraction evolves similarly in the CRP for all systems. As above mentioned the liquid fraction in small pores evolves differently depending on the connection status of the large pores: for connected large pores  $\psi_2$  increases until the end of the main emptying phase of the large pores, while for nonconnected large pores  $\psi_2$  decreases more rapidly for a smaller initial amount of large pores.

Considering the simultaneous decrease of the saturation in the large and small pores, along with the observation that the sample contraction approximately ends when the large-pore draining is finished, we can roughly assume that during all this period the amount of liquid in the small pores decreases as a result of the matrix shrinkage,

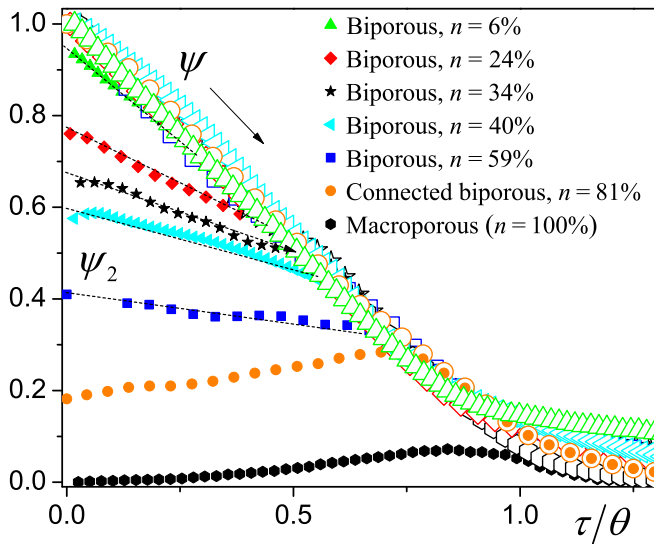


FIG. 11. Total liquid fraction (open large symbols) and liquid fraction in small pores (small filled symbols) and saturation in small pores times the initial fraction of small pores (small filled symbols) as a function of the rescaled time during drying for the different dispersed biporous structures (i.e., unconnected large pores), the connected biporous structure and the macroporous structure.

and proportionally to the current total amount of liquid. Moreover, due to the balance between the breakthrough capillary pressure and the material strength for the microporous matrix as described above, we expect that at the end of this period the small pores are contracted to the maximum value measured with the homogeneous microporous sample (see Fig. 2), i.e., by a factor of about 0.75. Under these conditions  $\psi_2$  initially equal to  $(1 - n)$  by definition, should evolve linearly to  $0.75(1 - n)$ . We can see that this model describes very well the data (see Fig. 11).

We finally can present a general scheme of the different characteristics of drying of biporous systems as a function of their structure properties, for partial wetting conditions (contact angle below  $90^\circ$ ) between the liquid and the solid phase and negligible gravity effects. Under these conditions, in all cases a long CRP should be observed.

(1) For connected large pores the drying essentially develops in the form of air finger progressively advancing in the large-pore network, and shrinkage is generally negligible. Then the small-pore matrix dries and can shrink under the action of capillary effects if it is compressible.

(2) For nonconnected large pores the liquid is extracted from these pores first while the small-pore matrix remains saturated. During this process, if the system is

compressible the large pores can shrink all the more as their concentration is larger.

#### IV. CONCLUSION

We show that in a compressible biporous medium with dispersed large pores (i.e., not directly connected) drying induces the emptying of the large pores first, due to their compression, along with some compression of the small-pore matrix. In contrast, when the large pores are connected, the large pores successively empty without compression. In both cases, the small pores start or finish to empty in the second stage, during which a CRP is observed during most of the time, thanks to liquid films maintaining the contact of the liquid network with the free surface of the sample. These results show that whatever the porous structure (connected, unconnected, or even dilute, dispersed large pores in a matrix of small pores) the largest pores homogeneously fully drain first during the CRP, while the small pores partially drain too, these effects being the results of contraction.

As the origin of this mechanism is the capillary balance throughout the sample at any time during the CRP, we can attempt to extrapolate this result to any pore size distribution, which tells us that the largest pores will tend to fully drain first as a result of compression. However, we have also seen that, for dispersed large pores, the surrounding small pores must partially drain at the same time. This implies that for a porous medium made of a continuous range of pore sizes we hardly distinguish some initial draining of the largest pores since at any step of draining (the largest pores) a significant fraction of the other pores (and, in particular, the pores of size just below the largest ones) would be emptied.

These elements provide some means to control drying characteristics in applications: it may appear useful to place large pores filled with liquid, which will dry first and shrink during drying; the connectivity between large pores should be chosen as a function of the expected compression during drying. For example, our results show that a sponge, i.e., a rather soft solid, made of connected large pores will not shrink significantly during drying while a sponge with nonconnected large pores will shrink.

It is also worth emphasizing that these results are obtained thanks to a powerful technique, i.e., NMR relaxometry, allowing to directly obtain measurements of the amount of liquid in the different pore types of the materials during drying. Other imaging techniques essentially provide either global information on the liquid content or detailed information at the pore scale, which are then difficult to extrapolate at a larger scale. Note however that NMR relaxometry is valuable when the material properties are favorable, which here means that the relaxation times of the liquid in its different states (or pores) are not too close.

## APPENDIX A: MERCURY INTRUSION POROSIMETRY

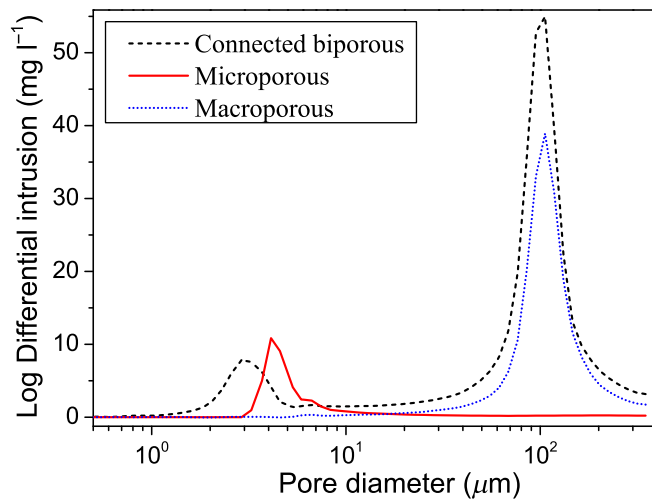


FIG. 12. Mercury porosimetry intrusion profiles for different samples (data from [22]).

## APPENDIX B: SAMPLE CONTRACTION

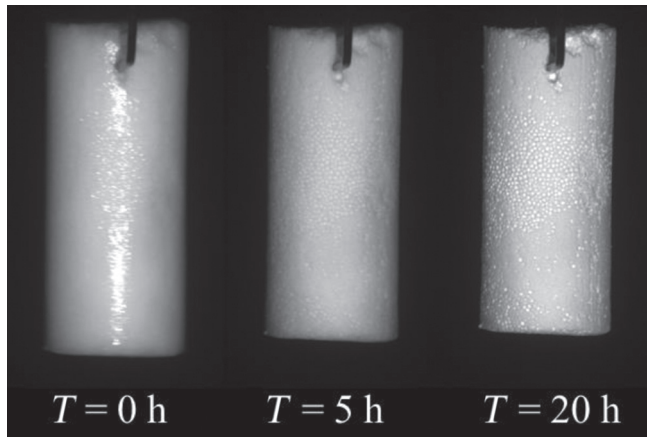


FIG. 13. Aspect of a (long) biporous material ( $n = 0.45$ ) at different times during drying. Initial diameter: 12 mm.

- [1] J. Van Brakel, in *Advances in Drying*, edited by Mujumdar A. S. (Hemisphere Pub. Corp., New York, 1980), Vol. 1, pp. 217–267.
- [2] J. B. Laurindo and M. Prat, Numerical and experimental network study of evaporation in capillary porous media. drying rates, *Chem. Eng. Sci.* **53**, 2257 (1998).
- [3] I. N. Tsimpanogiannis, Y. C. Yortsos, S. Poulou, N. Kanellopoulos, and A. K. Stubos, Scaling theory of drying in porous media, *Phys. Rev. E* **59**, 4353 (1999).

- [4] P. Coussot, Scaling approach of the convective drying of a porous medium, *Eur. Phys. J. B* **15**, 557 (2000).
- [5] J. Thiery, S. Rodts, D. A. Weitz, and P. Coussot, Drying regimes in homogeneous porous media from macro- to nanoscale, *Phys. Rev. Fluids* **2**, 074201 (2017).
- [6] L. Xu, S. Davies, A. B. Schofield, and D. A. Weitz, Dynamics of Drying in 3D Porous Media, *Phys. Rev. Lett.* **101**, 094502 (2008).
- [7] L. Pel, H. Brocken, and K. Kopinga, Determination of moisture diffusivity in porous media using moisture concentration profiles, *Int. J. Heat Mass Transfer* **39**, 1273 (1996).
- [8] V. Voronina, L. Pel, and K. Kopinga, Effect of osmotic pressure on salt extraction by a poultice, *Constr. Build. Mater.* **53**, 432 (2014).
- [9] M. D. Seck, E. Keita, P. Faure, P. Cavalié, M. Van Landeghem, S. Rodts, and P. Coussot, Subflorescence and plaster drying dynamics, *Chem. Eng. Sci.* **148**, 203 (2016).
- [10] P. Faure and P. Coussot, Drying of a model soil, *Phys. Rev. E* **82**, 036303 (2010).
- [11] D. Or, P. Lehmann, E. Shahraeeni, and N. Shokri, Advances in soil evaporation physics-A review, *Vadose Zone J.* **12**, 1 (2013).
- [12] N. Shokri and D. Or, What determines drying rates at the onset of diffusion controlled stage-2 evaporation from porous media?, *Water Resour. Res.* **47**, W09513 (2011).
- [13] P. Coussot, C. Gauthier, D. Nadji, J. C. Borgotti, P. Vié, and F. Bertrand, Capillary motions during the drying of a granular pastes, *C.R. Acad. Sci., Paris* **327**, 1101 (1999).
- [14] N. Ben Abdelouahab, A. Gossard, S. Rodts, B. Coasne, and P. Coussot, Convective drying of a porous medium with a paste cover, *Eur. Phys. J. E* **5**, 66 (2019).
- [15] G. W. Scherer, Recent progress in drying of gels, *J. Non-Cryst. Solids* **14è-148**, 363 (1992).
- [16] J. Thiery, E. Keita, S. Rodts, D. Courtier Murias, T. Kodger, A. Pegoraro, and P. Coussot, Drying kinetics of deformable and cracking nano-porous gels, *Eur. Phys. J. E* **39**, 117 (2016).
- [17] J. Thiery, S. Rodts, E. Keita, X. Chateau, P. Faure, D. Courtier-Murias, T. E. Kodger, and P. Coussot, Water transfer and crack regimes in nanocolloidal gels, *Phys. Rev. E* **91**, 042407 (2015).
- [18] L. Yang and H. H. Liu, A review of eucalyptus wood collapse and its control during drying, *Bioresources* **13**, 2171 (2018).
- [19] M. P. Milner, L. Jin, and S. B. Hutchens, Creasing in evaporation-driven cavity collapse, *Soft Matter* **13**, 6894 (2017).
- [20] J. Rey and M. Vandamme, On the shrinkage and stiffening of a cellulose sponge upon drying, *J. Appl. Mech.* **80**, 020908 (2013).
- [21] H. B. Ly, B. Le Droumaguet, V. Monchiet, and D. Grande, Facile fabrication of doubly porous polymeric materials with controlled nano- and macro-porosity, *Polymer* **78**, 13 (2015).
- [22] T. Lerouge, P. Pitois, D. Grande, B. Le Droumaguet, and P. Coussot, Synergistic actions of mixed small and large pores for capillary absorption through biporous polymeric materials, *Soft Matter* **14**, 8137 (2018).

- [23] S. Mezhoud, PhD thesis, Univ. Paris-Est, 2018.
- [24] E. Keita, S. A. Koehler, P. Faure, D. A. Weitz, and P. Coussot, Drying kinetics driven by the shape of the air/water interface in a capillary channel, *Eur. Phys. J. E* **39**, 23 (2016).
- [25] K. P. Whittall and A. L. MacKay, Quantitative interpretation of NMR relaxation data, *J. Magn. Reson.* **84**, 134 (1989).
- [26] S. W. Provencher, A constrained regularization method for inverting data represented by linear algebraic or integral equations, *Comput. Phys. Commun.* **27**, 213 (1982).
- [27] P. Faure and S. Rodts, Proton NMR relaxation as a probe for setting cement pastes, *Magn. Reson. Imaging* **26**, 1183 (2008).
- [28] S. Philippot, J. P. Korb, D. Petit, and H. Zanni, Analysis of microporosity and setting of reactive powder concrete by proton nuclear relaxation, *Magn. Reson. Imaging* **16**, 515 (1998).
- [29] K. R. Brownstein and C. E. Tarr, Spin-lattice relaxation in a system governed by diffusion, *J. Magn. Reson.* **26**, 17 (1977).
- [30] C. Chen, P. Joseph, S. Geoffroy, M. Prat, and P. Duru, Evaporation with the formation of chains of liquid bridges, *J. Fluid Mech.* **837**, 703 (2018).
- [31] F. Chauvet, P. Duru, S. Geoffroy, and M. Prat, Three Periods of Drying of a Single Square Capillary Tube, *Phys. Rev. Lett.* **103**, 124502 (2009).
- [32] M. D. Seck, E. Keita, and P. Coussot, Some observations on the impact of a low solubility ionic solution on drying characteristics of a model porous medium, *Transp. Porous Media* **128**, 915 (2019).
- [33] S. Biswas, P. Fantinel, O. Borgman, R. Holtzman, and L. Goehring, Drying and percolation in correlated porous media, *Phys. Rev. Fluids* **3**, 124307 (2018).
- [34] M. Prat, Percolation model of drying under isothermal conditions in porous media, *Int. J. Multiphase Flow* **19**, 691 (1993).
- [35] T. M. Shaw, Drying as an Immiscible Displacement Process with Fluid Counterflow, *Phys. Rev. Lett.* **59**, 1671 (1987).
- [36] R. Wu, C. Y. Zhao, E. Tsotsas, and A. Kharaghani, Convective drying in thin hydrophobic porous media, *Int. J. Heat Mass Transfer* **112**, 630 (2017).
- [37] K. M. Pillai, M. Prat, and M. Marcoux, A study on slow evaporation of liquids in a dual-porosity porous medium using square network model, *Int. J. Heat Mass Transfer* **52**, 1643 (2009).
- [38] A. G. Yiotis, A. G. Boudouvis, A. K. Stubos, N. Tsimpanogiannis, and Y. C. Yortsos, Effect of liquid films on the drying of porous media, *AIChE J.* **50**, 2721 (2004).
- [39] L. Landau and E. Lifchitz, *Théorie de L'élasticité* (Editions Mir, Moscou, 1967).